The Environmental Story During the COVID-19 Lockdown: How Human Activities Affect PM2.5 Concentration in China?

Zhenyu Tan, Xinghua Li, *Member, IEEE*, Meiling Gao, and Liangcun Jiang

***Abstract*— At the end of 2019, the very first COVID-19 coronavirus infection was reported and then it spread across the world just like wildfires. From late January to March 2020, most cities and villages in China were locked down, and consequently, human activities decreased dramatically. This letter presents an "offline learning and online inference" approach to explore the variation of PM2.5 pollution during this period. In the experiments, a deep regression model was trained to establish the complex relationship between remote sensing data and *in situ* PM2.5 observations, and then the spatially continuous monthly PM2.5 distribution map was simulated using the Google Earth Engine platform. The results reveal that the COVID-19 lockdown truly decreased the PM2.5 pollution with certain hysteresis and the fine particle pollution begins to increase when advancing resumption of work and production gradually.**

***Index Terms*— Absorbing Aerosol Index (AAI), Aerosol Optical Depth (AOD), COVID-19, deep learning, Google Earth Engine (GEE), PM2.5, remote sensing.**

I. Introduction

IN DECEMBER 2019, a novel coronavirus disease, named COVID-19, was reported in Wuhan, China, and soon outbroke all over the world rapidly [1], [2]. COVID-19 is highly contagious [3] and causes a large number of deaths [4]. After the outbreak of COVID-19, the Wuhan government locked the city down on January 23, 2020, to prevent further spreading, and other cities across the country were forced to be under lockdown in quick succession. The government advocated citizens to stay at home to lessen infections and deaths. Under this circumstance, most of the production activities were halted and outdoor activities were dramatically decreased. The resumption of production has been taking place since March 2020. At the end of April, most of the major industries restarted their production, and people's lives gradually returned to normalcy.

This nationwide lockdown led to a short period of time during which human activities were diminished significantly. Generally, human activities are actively involved in the global atmospheric circulation, showing a substantial impact on ambient air quality [5]. The small liquid and solid particles suspending in the air, referred to as particulate matter, have become a major component of atmospheric pollutants [6]. Particulate matter is usually detrimental to human beings, especially the fine particles with a diameter of less than 2.5 μm, known as PM2.5 [7]. Because the PM2.5 can cause a severe threat to human health [8], or even death [9], many studies focus on the interaction between human health and PM2.5 [10], [11], as well as the impact of PM2.5 on human health [8], [12]. This letter, taking China as an example, dedicates to exploring the spatial and temporal distribution variation of PM2.5 concentration when human activities decreased dramatically.

By utilizing the deep learning technology and multisource remote sensing data via Google Earth Engine (GEE) platform, this work demonstrates a convenient and efficient approach to explore the influence of human activities on ambient PM2.5. This letter is organized as follows. The background is introduced in Section I. Section II presents the employed data and model for the spatially continuous PM2.5 simulation. The experiments and results are provided in Section III. Section IV is the summary and conclusion.

II. Materials and Methods

A. Data Sets for PM2.5 Concentration Simulation

Currently, the PM2.5 concentration can be observed directly from *in situ* air quality monitoring stations. However, discretely distributed *in situ* observations cannot fully describe spatially continuous distribution over the entire study area. Remote sensing, to the contrary, can be employed to derive spatially continuous PM2.5 concentration with certain accuracy [13], [14]. Some studies show that several substances are relevant to the generation of PM2.5, such as road dust, mineral dust, and vehicle exhaust [15], [16], and human activities can contribute to the generation of this harmful aerosol. Accordingly, researchers use multisource remote sensing data sets to perform the simulation of PM2.5 concentration distribution [17], [18]. The Aerosol Optical Depth (AOD), as one of the key factors relevant to PM2.5, measures the amount of aerosol particles in the atmosphere, such as dust, smoke, and pollution. It is often derived from remote sensing data and shows a quite strong correlation with PM2.5 concentration, thus, it is extensively utilized to simulate the distribution of PM2.5 concentration [19], [20].

Manuscript received June 3, 2020; revised September 18, 2020; accepted November 21, 2020. Date of publication December 8, 2020; date of current version December 15, 2021. This work was supported by the National Natural Science Foundation of China under Grant 41901315. *(Corresponding author: Xinghua Li.)*

Zhenyu Tan is with the College of Urban and Environmental Sciences, Northwest University, Xi'an 710127, China (e-mail: tanzhenyu@nwu.edu.cn).

Xinghua Li and Liangcun Jiang are with the School of Remote Sensing and Information Engineering, Wuhan University, Wuhan 430079, China (e-mail: lixinghua5540@whu.edu.cn).

Meiling Gao is with the School of Geology Engineering and Geomatics, Chang'an University, Xi'an 710054, China.

Digital Object Identifier 10.1109/LGRS.2020.3040435

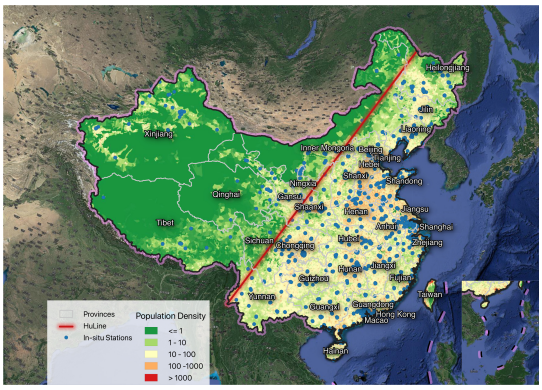

Fig. 1. Study area and *in situ* observation stations.

In this letter, first of all, a deep learning regression model is established to map the corresponding pixel values picked up from multisource remote sensing data to the discrete *in situ* PM2.5 observations in a point-to-point manner. Then the trained model is transferred for the remote sensing images to simulate the spatially continuous PM2.5 distribution. The hourly *in situ* observations were collected from the city air quality publishing platform of China National Environmental Monitoring Centre (CNEMC) and averaged to produce daily measurements for model training. Fig. 1 illustrates the *in situ* monitoring stations in the study area. The ultimate goal of this letter is to explore how human activities affected ambient PM2.5 concentration in China during the COVID-19 lockdown, therefore, it is significantly important to know the population distribution of the study area. The background color of the study area in Fig. 1 indicates the estimated number of people per square kilometer in 2020. The Hu Line in red named after a famous Chinese geographer visually shows that China possesses a dense population southeast and sparse population northwest. In the following experiment analysis, the PM2.5 variation in the two different population zones may be separated in some discussion to probe how the decreased human activities affected the ambient PM2.5 concentration.

Two different kinds of remote sensing data sets are acquired for the experiments. First of all, the daily MODIS AOD product (MCD19A2) with the spatial resolution of 1 km is primarily chosen to be involved in the simulation. Two AOD data layers in the MCD19A2 data set are both used, and they are derived from blue (0.47 μm) and green (0.55 μm) spectral bands. Second, the Absorbing Aerosol Index (AAI) band of the Ultraviolet Aerosol Index product (Sentinel-5P OFFL AER AI) is experimentally added to the model to explore possible improvements. The employed daily AAI is derived from the Sentinel-5P satellite using the 354 nm/388 nm wavelength pair with the spatial resolution of 0.01 arc degrees. It indicates the presence of estimated absorbing aerosols, including desert dust and biomass burning aerosols, and so on. The data need to be resampled to gain the same resolution with MCD192A images. All the remote sensing data sets come from the GEE cloud platform. The GEE not only provides a massive amount of archived satellite imagery but also enables large scale analysis capabilities based on Google's cloud infrastructure. All the data collection, preprocessing, and model inference can be performed on GEE in the cloud in a distributed parallel processing manner, which means it will save much more time than the conventional way.

B. Deep Learning Approach for PM2.5 Simulation

Several models have been proposed over the past few years to simulate the spatially continuous PM2.5 concentration, such as the simple linear regression [21], geographically weighted regression [22], statistical models [23], machine learning models [24], deep learning models [25], and ensemble models [26]. Among them, deep-learning-based models have gained much more attention in recent years due to the higher accuracy compared with other conventional models [27]. A deep learning model learns from massive data automatically without handcrafted rules, naturally suitable for modeling with various inputs in the PM2.5 simulation problem.

This letter presents an "offline learning and online inference" deep learning approach for PM2.5 concentration simulation. Specifically, the designed deep neural network consists of three hidden layers and each layer shares the same structure composing of a simple linear transformation and nonlinear activation, formulated as (1) and (2). In the equations, f_i denotes the transformations in the ith layer with the inputs $\boldsymbol{x}_i$. $\boldsymbol{A}_i$ and $\boldsymbol{b}_i$ are the learnable parameters of the ith layer. The activation after the linear transformation is the rectified linear units (ReLU), which is an efficient and effective nonlinear function, commonly used in deep models. The $F(\boldsymbol{x_1})$ denotes the deep regression model with the initial input data $\boldsymbol{x_1}$. Data flow the hidden layers sequentially, and finally, the prediction is generated by the last model layer. The inputs of this regression model are the picked-up pixel values corresponding to the *in situ* stations from the multisource remote sensing data, and the output is the *in situ* observed PM2.5 observations for supervised training. The input channels depend on the number of input data sources, for instance, if AOD data from blue and green bands are served as the inputs, then the input channel is two; if AOD and AAI data are entered into the model together, then the input channel should be three. The output channel of each hidden layer is the hyperparameter and should be determined before training. The channels of the three hidden layers are set to 16, 32, and 1 experimentally in our simulations. The output channel of the last hidden layer is equal to one because the model output only includes one observation feature, namely the PM2.5 concentration

$$f_i(\boldsymbol{x}_i) = \text{ReLU}\left(\boldsymbol{x}_i \boldsymbol{A}_i^{\mathrm{T}} + \boldsymbol{b}_i\right) \tag{1}$$

$$F(\boldsymbol{x_1}) = f_3(f_2(f_1(\boldsymbol{x_1}))). \tag{2}$$

Since the GEE platform currently does not support online training for deep models, and the size of our model is quite small, an "offline learning and online inference" approach is applied to perform the experiments. All the procedures are illustrated as Fig. 2, where the processing boxes in blue indicate offline operations and the green boxes denote online operations using GEE. To be specific, the PM2.5 observations from monitoring stations should be collected at first, and then the related remote sensing pixel values including the AOD and AAI should be acquired from GEE archived imagery according

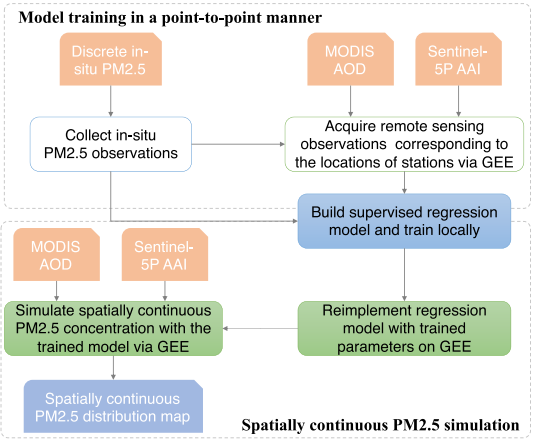

Fig. 2. "Offline learning and online inference" flowchart.

to the corresponding locations of observation points. Second, the regression model should be trained locally using the back-propagation algorithm with the inputs of the picked-up remote sensing pixels and the output of the *in situ* observations. Third, the learnable parameters of the trained model are extracted, and the regression process needs to be reimplemented on GEE with the learned parameters. Finally, the relevant remote sensing images, including MODIS AOD and Sentinel-5P AAI, are entered into the reimplemented online model to generate the spatially continuous PM2.5 simulation via GEE.

III. Experiments and Results

A. Experiments

After collecting the *in situ* observations from monitoring stations and acquiring the remote sensing pixel values in the corresponding locations via GEE, these data points were grouped for training. There are a total of 22 750 data pairs collected from December 2019 to April 2020. Seventy percent of them were used for training and the rest for validation. It is worth mentioning that because the multisource input data sets have different value range, they need to be normalized to a unit scale. In the following experiments, (3) was used to scale the inputs to bring all values into the range [0, 1], where x_i is the ith feature value of the remote sensing data set $\boldsymbol{x}$; $x_{\min}$ and $x_{\max}$ denote the minimum and maximum values of the $\boldsymbol{x}$. MODIS AOD and its combination with Sentinel-5P AAI were both tested in the training stage to explore their performance. With the aforementioned model setting, after 10 000 epochs training, the evaluation results on the validation data set are summarized in Table I. Mean absolute error (MAE), Coefficient of Determination (R^2), and Pearson correlation coefficient (CC) metrics are used to measure the performance. The MAE is around 17 $\mu g/m^3$ for the two experiment groups, which is enough for later simulation considering the wide value range of PM2.5 concentration over the study area. The CC is greater than 0.5 showing a moderate correlation between prediction and observation, which is also acceptable for variation trend analysis. The combination of MODIS AOD and Sentinel-5P AAI data for model input outperforms the one with single AOD from the perspective of R^2 and CC. Fig. 3 illustrates the correlation between *in situ* observations and simulated

TABLE I
Evaluation Results With Different Model Inputs

Training group	Learnable parameters	MAE	R^2	CC
MODIS AOD	625	17.500	0.319	0.565
AOD & AAI	641	17.131	0.408	0.641

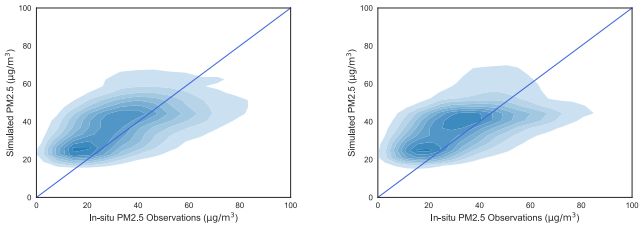

(a) (b)

Fig. 3. Fitness estimation for model simulation. (a) Simulation with AOD. (b) Simulation with AOD and AAI.

results on validation data set using kernel density estimation. The shades of the color indicate the density. It can intuitively demonstrate how the simulated PM2.5 concentration fits the actual observation. Perceptually, the simulation with the combination of AOD and AAI is more closed to the blue identify line. Hence, the AOD and AAI data are both used for the spatially continuous PM2.5 concentration simulation. The simulation was performed on the monthly averaged images considering the frequent data missing of MODIS observations and the slow variation of daily PM2.5 concentration

$$x_i := \frac{x_i - x_{\min}}{x_{\max} - x_{\min}}. \tag{3}$$

B. Results and Analysis

Fig. 4 demonstrates the simulated results as well as the monthly averaged *in situ* observations from December 2019 to April 2020. Also, Fig. 5 exhibits the previous year's PM2.5 concentration of the same period from December 2018 to April 2019 to facilitate the comparison. The color of the map indicates the simulated monthly-averaged PM2.5 concentration. Blank color represents missing data in the original remote sensing images. Several phenomena can be observed from Figs. 4 and 5.

1) An abnormal increase occurred in Xinjiang in March and April 2020. We believe this is caused by seasonal sand and dust storms (SDS) because there are wild tracts of desert in Xinjiang and the SDS happens in spring frequently according to the literature [28], [29]. Besides, the simulation results from March 2019 to April 2019 in Fig. 5 also confirm this conjecture.
2) January 2020 just before the lockdown exhibited moderate PM2.5 pollution for the southeast provinces with a dense population. After the large-scale lockdown, the PM2.5 concentration showed a significant reduction in February 2020. It reveals that the dramatic decrease in human production and activities can truly lead to a reduction in PM2.5 generation. Moreover, the PM2.5 concentration in February 2019 is rather higher

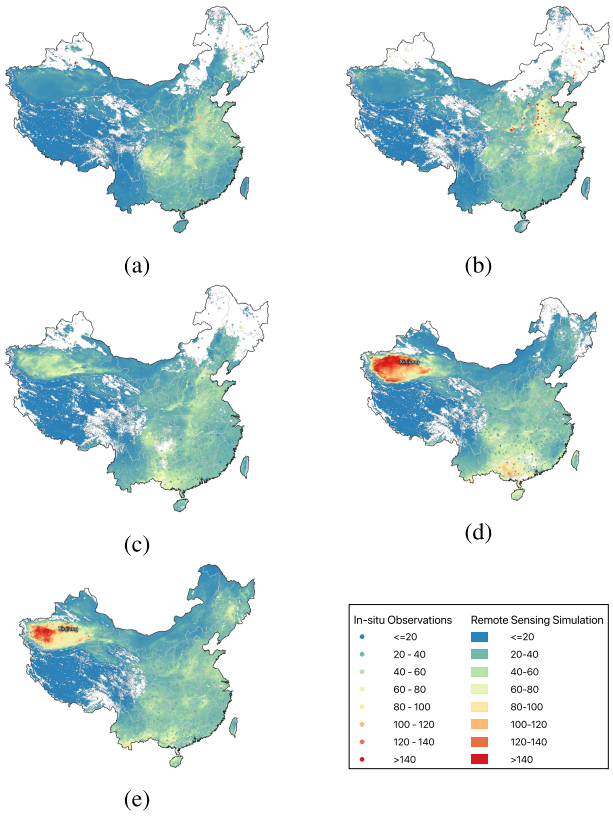

Fig. 4. Simulated monthly-averaged PM2.5 concentration from December 2019 to April 2020. (a) December 2019. (b) January 2020. (c) February 2020. (d) March 2020. (e) April 2020.

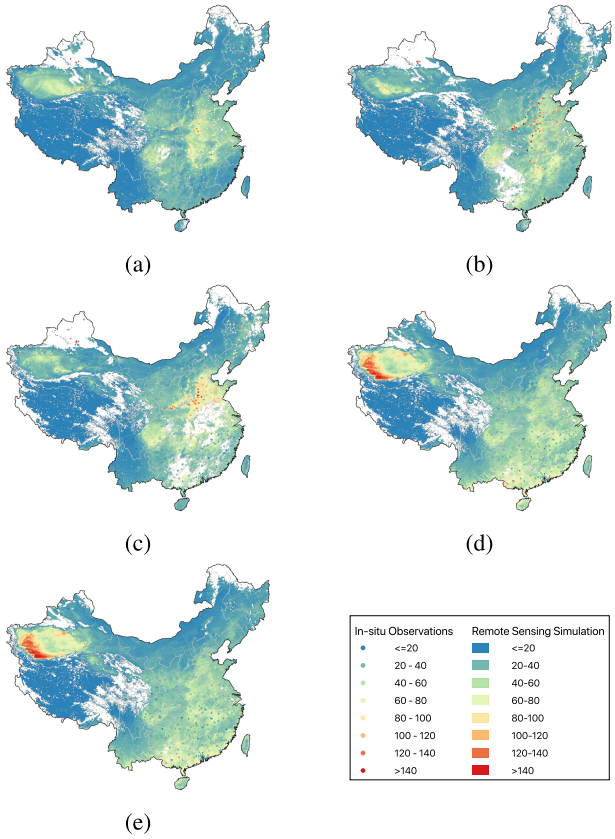

Fig. 5. Simulated monthly-averaged PM2.5 concentration from December 2018 to April 2019. (a) December 2018. (b) January 2019. (c) February 2019. (d) March 2019. (e) April 2019.

than simulated in February 2020. This, from another perspective, shows the PM2.5 pollution weakened during the lockdown. This phenomenon also conforms to the conclusion that the PM2.5 concentration declines over major cities around the world during the COVID-19 lockdown [30].

3) March 2020 had the lowest PM2.5 pollution since the COVID-19 lockdown except for Xinjiang and Guangxi regions. The lockdown began at the end of January 2020, while the lowest PM2.5 pollution happened in March for most of the regions when people had gradually resumed production. This phenomenon confirms the common hysteresis effect of human activities on the air [31]. The air requires some time to do self-cleaning, even though the pollutant emission is reduced dramatically. Besides, the PM2.5 concentration from March and April 2020 is lower than that of the same period in the previous year. In other words, the PM2.5 pollution can maintain a quite low level after the work resumption, which, again, shows the existence of the hysteresis effect.

Fig. 6 demonstrates the PM2.5 variation month to month over the study area quantitatively. Some conclusions can be drawn from this chart.

1) The PM2.5 concentration in the eastern area of Hu Line observed from remote sensing and *in situ* stations have the same varying tendency with different magnitude. Considering the nonuniformity and sparsity of the station distribution, as well as the abnormal increase in Xinjiang, the simulated results can be considered to conform with the *in situ* observations. Two lines from the *in situ* observations almost overlapped because there are rather fewer minoring stations distributed in the western area of Hu Line and the variations of these areas cannot be measured completely.

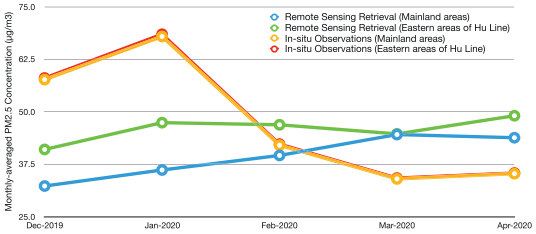

Fig. 6. Monthly-averaged PM2.5 concentration over the study area (the remote sensing derived PM2.5 concentration is the aggregated mean for the entire study area).

2) From the simulation statistics in the eastern area of Hu Line where a majority of people live, there was an obvious decrease after the lockdown. The growth rate observed from remote sensing derived PM2.5 for the eastern area of Hu Line is -1.07% from January to February and -4.62% from February to March. These numbers also confirm the aforementioned hysteresis effect of atmospheric circulation. However, being affected by the abnormal increase in Xinjiang,

the simulated PM2.5 during the first quarter of 2020 over the entire study area is increased slightly.

3) According to the simulation results, the PM2.5 concentration was still decreasing in April 2020 all over the entire study area, but the PM2.5 pollution increased by 9.67% regarding the eastern area of Hu Line. The decrease for the entire study area may be due to the partially reduced PM2.5 in Xinjiang, and the increase in the southeast may be caused by the large-scale work resumption.

IV. Conclusion

The COVID-19 coronavirus was first emerged at the end of 2019 and outbroke all over the world quickly, causing severe losses for the human being. From late January to March 2020, the governments are forced to lock down some cities to prevent further infections. This letter devotes to explore the variation of PM2.5 pollution during the period when human production and activities are diminished dramatically. To this end, an "offline learning and online inference" approach is applied to train a deep regression model between multisource remote sensing data and the *in situ* PM2.5 observations, and then it is used to perform spatially continuous PM2.5 concentration simulation using the GEE platform. The experiments show that the combination of MODIS AOD and Sentinel-5P AAI data can improve the PM2.5 simulation accuracy.

From the simulation results and *in situ* observations, January 2020 just before the lockdown has the worst PM2.5 pollution in China, and the fine particle pollution reduces significantly after the large-scale lockdown. The lowest averaged PM2.5 concentration is observed in March, showing an evident hysteresis effect. When people going back to work gradually, the PM2.5 pollution begins to increase in Eastern China in April 2020, but still lower than that in April 2019. In a nutshell, the lockdown in China during the COVID-19 contributes to the decrease of PM2.5 pollution with certain hysteresis.

References

[1] N. Chen *et al.*, "Epidemiological and clinical characteristics of 99 cases of 2019 novel coronavirus pneumonia in Wuhan, China: A descriptive study," *Lancet*, vol. 395, no. 10223, pp. 507–513, Feb. 2020.

[2] A. Remuzzi and G. Remuzzi, "COVID-19 and Italy: What next?" *Lancet*, vol. 395, no. 10231, pp. 1225–1228, Apr. 2020.

[3] Y.-Y. Zheng, Y.-T. Ma, J.-Y. Zhang, and X. Xie, "COVID-19 and the cardiovascular system," *Nature Rev. Cardiol.*, vol. 17, no. 5, pp. 259–260, 2020.

[4] D. Baud, X. Qi, K. Nielsen-Saines, D. Musso, L. Pomar, and G. Favre, "Real estimates of mortality following COVID-19 infection," *Lancet Infectious Diseases*, vol. 20, no. 7, p. 773, Jul. 2020.

[5] A. Salic and B. Zelic, "Introduction to environmental engineering," *Phys. Sci. Rev.*, vol. 3, no. 3, 2018, p. 20160115.

[6] C. I. Davidson, R. F. Phalen, and P. A. Solomon, "Airborne particulate matter and human health: A review," *Aerosol Sci. Technol.*, vol. 39, no. 8, pp. 737–749, Aug. 2005.

[7] L. L. Sloss and I. M. Smith, "PM_{10} and $PM_{2.5}$: An international perspective," *Fuel Process. Technol.*, vols. 65–66, pp. 127–141, Jun. 2000.

[8] C. Song *et al.*, "Health burden attributable to ambient $PM_{2.5}$ in China," *Environ. Pollut.*, vol. 223, pp. 575–586, Apr. 2017.

[9] S. Chowdhury and S. Dey, "Cause-specific premature death from ambient $PM_{2.5}$ exposure in India: Estimate adjusted for baseline mortality," *Environ. Int.*, vol. 91, pp. 283–290, May 2016.

[10] S. Wang, X. Liu, X. Yang, B. Zou, and J. Wang, "Spatial variations of $PM_{2.5}$ in Chinese cities for the joint impacts of human activities and natural conditions: A global and local regression perspective," *J. Cleaner Prod.*, vol. 203, pp. 143–152, Dec. 2018.

[11] L. Han, W. Zhou, W. Li, and L. Li, "Impact of urbanization level on urban air quality: A case of fine particles ($PM_{2.5}$) in Chinese cities," *Environ. Pollut.*, vol. 194, pp. 163–170, 2014.

[12] F. Lu *et al.*, "Systematic review and meta-analysis of the adverse health effects of ambient $PM_{2.5}$ and PM_{10} pollution in the Chinese population," *Environ. Res.*, vol. 136, pp. 196–204, Jan. 2015.

[13] A. V. R. V. Donkelaar Martin and R. J. Park, "Estimating ground-level $PM_{2.5}$ using aerosol optical depth determined from satellite remote sensing," *J. Geophys. Res., Atmos.*, vol. 111, no. D21, pp. 1–10, 2006, doi: 10.1029/2005JD006996.

[14] Z. Ma, X. Hu, L. Huang, J. Bi, and Y. Liu, "Estimating ground-level $PM_{2.5}$ in China using satellite remote sensing," *Environ. Sci. Technol.*, vol. 48, no. 13, pp. 7436–7444, 2014.

[15] S. Rodrlguez *et al.*, "Comparative PM10–$PM_{2.5}$ source contribution study at rural, urban and industrial sites during PM episodes in Eastern Spain," *Sci. Total Environ.*, vol. 328, no. 1, pp. 95–113, 2004.

[16] D. Xia, B. Jiang, and Y. Xie, "Modeling and analysis of $PM_{2.5}$ generation for key factors identification in China," *Atmos. Environ.*, vol. 134, pp. 208–216, Jun. 2016.

[17] X. Y. Ni, H. Huang, and W. P. Du, "Relevance analysis and short-term prediction of $PM_{2.5}$ concentrations in Beijing based on multi-source data," *Atmos. Environ.*, vol. 150, pp. 146–161, Feb. 2017.

[18] F. Biancofiore *et al.*, "Recursive neural network model for analysis and forecast of PM_{10} and $PM_{2.5}$," *Atmos. Pollut. Res.*, vol. 8, no. 4, pp. 652–659, Jul. 2017.

[19] J. Wang and S. A. Christopher, "Intercomparison between satellite-derived aerosol optical thickness and $PM_{2.5}$ mass: Implications for air quality studies," *Geophys. Res. Lett.*, vol. 30, no. 21, pp. 1–4, 2003, doi: 10.1029/2003GL018174.

[20] Y. Xie, Y. Wang, K. Zhang, W. Dong, B. Lv, and Y. Bai, "Daily estimation of ground-level $PM_{2.5}$ concentrations over Beijing using 3 km resolution MODIS AOD," *Environ. Sci. Technol.*, vol. 49, no. 20, pp. 12280–12288, 2015.

[21] A. P. K. Tai, L. J. Mickley, and D. J. Jacob, "Correlations between fine particulate matter ($PM_{2.5}$) and meteorological variables in the united states: Implications for the sensitivity of PM2.5 to climate change," *Atmos. Environ.*, vol. 44, no. 32, pp. 3976–3984, Oct. 2010.

[22] X. Hu *et al.*, "Estimating ground-level $PM_{2.5}$ concentrations in the southeastern U.S. using geographically weighted regression," *Environ. Res.*, vol. 121, pp. 1–10, Feb. 2013.

[23] W. Yu, Y. Liu, Z. Ma, and J. Bi, "Improving satellite-based $PM_{2.5}$ estimates in China using Gaussian processes modeling in a Bayesian hierarchical setting," *Sci. Rep.*, vol. 7, no. 1, p. 7048, 2017.

[24] A. Sotomayor-Olmedo, M. A. Aceves-Fernández, E. Gorrostieta-Hurtado, C. Pedraza-Ortega, J. M. Ramos-Arreguín, and J. E. Vargas-Soto, "Forecast urban air pollution in Mexico City by using support vector machines: A kernel performance approach," *Int. J. Intell. Sci.*, vol. 03, no. 03, pp. 126–135, 2013.

[25] C.-J. Huang and P.-H. Kuo, "A deep CNN-LSTM model for particulate matter ($PM_{2.5}$) forecasting in smart cities," *Sensors*, vol. 18, no. 7, p. 2220, Jul. 2018.

[26] L. Feng, Y. Li, Y. Wang, and Q. Du, "Estimating hourly and continuous ground-level $PM_{2.5}$ concentrations using an ensemble learning algorithm: The ST-stacking model," *Atmos. Environ.*, vol. 223, Feb. 2020, Art. no. 117242.

[27] A. Y. Ayturan, A. Z. Cansu, and A. H. Oktay, "Air pollution modelling with deep learning: A review," *Int. J. Environ. Pollut. Environ. Model.*, vol. 1, no. 3, pp. 58–62, 2019.

[28] K. Hu, K. R. Kumar, N. Kang, R. Boiyo, and J. Wu, "Spatiotemporal characteristics of aerosols and their trends over mainland China with the recent collection 6 MODIS and OMI satellite datasets," *Environ. Sci. Pollut. Res.*, vol. 25, no. 7, pp. 6909–6927, Mar. 2018.

[29] M. Filonchyk, H. Yan, S. Yang, and X. Lu, "Detection of aerosol pollution sources during sandstorms in northwestern China using remote sensed and model simulated data," *Adv. Space Res.*, vol. 61, no. 4, pp. 1035–1046, Feb. 2018.

[30] A. Chauhan and R. P. Singh, "Decline in PM2.5 concentrations over major cities around the world associated with COVID-19," *Environ. Res.*, vol. 187, Aug. 2020, Art. no. 109634.

[31] J. Wang, A. A. Hoffmann, R. J. Park, D. J. Jacob, and S. T. Martin, "Global distribution of solid and aqueous sulfate aerosols: Effect of the hysteresis of particle phase transitions," *J. Geophys. Res.*, vol. 113, no. D11, pp. 1–11, 2008, doi: 10.1029/2007JD009367.